IEEE Access
Multidisciplinary | Rapid Review | Open Access Journal

Received May 11, 2020, accepted June 18, 2020, date of publication June 23, 2020, date of current version July 1, 2020.

*Digital Object Identifier 10.1109/ACCESS.2020.3004365*

# Design of a Roll Angle Measuring Sensor

**WENCHANG YANG[1,2], ZHIQIAN WANG[1], CHENGWU SHEN[1,2], YUSHENG LIU[1,2], AND SHAOJIN LIU[1]**

[1]Changchun Institute of Optics, Fine Mechanics and Physics, Chinese Academy of Sciences, Changchun 130033, China
[2]University of Chinese Academy of Sciences, Beijing 100049, China

Corresponding author: Zhiqian Wang (wangzhiqian@ciomp.ac.cn)

This work was supported in part by the Jilin Provincial Major Project of China under Grant 20190302086GX and Grant 20200403067SF.

**ABSTRACT** Aiming at the measurement of roll deformation between two devices, we propose a novel scheme and elaborate the structure design in this paper. The scheme can realize the relative measurement of roll angle even if the system does not provide a reference datum, which effectively solves the problems of limited measurement range of moiré fringes and accuracy guarantee only in an extremely small angle range. First, the principle of measuring the roll angle by moiré fringes is introduced, and the effects of various error sources in the system are comprehensively considered. Then, the combined measurement scheme and the entire system composition structure are analyzed in detail. In addition, an experimental setup is designed to verify the accuracy of roll deformation measurement. The measurement results show that the root mean square (RMS) error can reach 6.9″ within 3°, and is less than 7.8″ in the range of 0°–90°. Hence, our proposed scheme has a good measurement stability in a large roll range.

**INDEX TERMS** Roll angle, measurement sensor, system structure design, error analysis, moiré fringe.

## I. INTRODUCTION

Angle sensors have been widely used in precise motion correction and other fields. Taking the ocean-going survey ships as an example, there are usually a variety of positional measurement and control systems such as radar, theodolite, and inertial navigation system (INS). External disturbances may cause three-dimensional (3D) angular deformation of the hull [1]–[3]. When other measurement devices use the reference datum from the inertial navigation system, large position errors are usually generated [3], [4]. In order to achieve error compensation and make the measurement result more accurate, it is necessary to measure the 3D angle between the bases of devices. The 3D angular deformation involves pitch, yaw, and roll [1], [2], [5]. The roll angle refers to the angular change of the center line of the device itself, which has an important practical engineering significance for the measurement of roll deformation [6], [7].

Nabergoj and Tondl [8] found in their experimental results that the roll deformation was as obvious as the pitch or yaw deformation. Since large angular deformation has an important impact on the accuracy of measurement instruments, many scholars have made a lot of efforts to the measurement of roll deformation [9]. In the contact measurement of roll angle, the shaft encoder has been widely used due to its remarkable advantages such as extremely high accuracy and reliable performance. The mainstream accuracy is less than 0.1″, and the error is almost negligible. With respect to the non-contact measurement, the optical method, such as polarized light measurement, self-collimation measurement, and visual measurement, has been widely used for its merits of high accuracy and high sensitivity. The principle of polarized light measurement is to install a polarimeter on the base of the reference device and a plane mirror with a polarizer on the base of the optical measurement device. The polarizer can emit a parallel beam that is then reflected by the mirror to produce a polarized light. If there is no roll between the devices, the luminous flux received by the polarimeter is a fixed value; otherwise the applied voltage can control the polarimeter to rotate by a certain angle. The angle at which the energy passed by it recovers its initial maximum value is the roll angle. This method requires a high uniformity of the polarimeter, and the RMS error is better than 5″ [10]. The self-collimating method is used to convert the roll angle into other two-dimensional angular deformations [11], [12]. TRIOPTICS developed a self-collimating instrument named TriAngle 3D, which had a resolution of 1″ and an accuracy of 5″ [13]. Yin *et al.* [13] proposed to integrate double gratings into a 3D self-collimation instrument, and the RMS error was 4.92″ in the 15'09″ roll range. The visual measurement method

The associate editor coordinating the review of this manuscript and approving it for publication was Wuliang Yin.

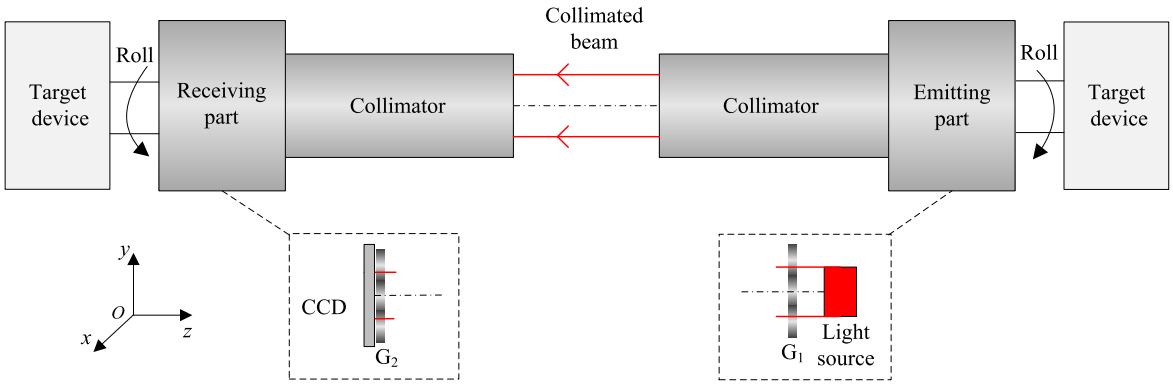


**FIGURE 1.** Schematic diagram of measuring roll angle with moiré fringes.

can calculate the roll angle according to the reconstructed torsion point array target [14]. Wei *et al.* [15] discovered that this scheme could realize visual torsional deformation measurement of large field, but had poor accuracy especially in dynamic scenes.

In this study, we propose a novel scheme for the measurement of roll angle, and the main contributions are as follows:

1) A non-contact roll measurement scheme using moiré fringes is proposed. We design the structure of the entire measurement sensor in detail, and analyze all error sources in the system. Moiré fringes can achieve relative measurement in a small angle range and do not depend on the system reference datum, which are suitable for the case where two devices roll each other. Compared with other schemes, non-reference measurement effectively reduces the impact of system reference errors.

2) Due to the effects of various error sources in the system, most schemes including moiré fringes have the problem that the measurement error increases rapidly with the increase of the range of roll angle measurement. In addition, when the roll angle is close to 0°, 90°, or 180°, the lack of effective moiré fringes in the field of view seriously affects the measurement robustness. In order to ensure the accuracy of roll angle measurement, we propose a novel model for combined measurement of roll angle. This scheme conducts the moiré fringe measurement within 10′, and adopts a shaft encoder with high stability and high accuracy above 10′. Finally, the accuracy of roll angle measurement is better than 7.8″. Therefore, this scheme effectively overcomes the problem of limited moiré fringe measurement range on the premise of ensuring the accuracy of roll angle.

The remainder of this paper is organized as follows. First, Section II introduces a non-contact measurement model of roll angle, and analyzes the error sources. Then, Section III presents the principle of combined measurement and parameters of main components. Further, an experimental setup is designed to verify the accuracy of roll angle measurement in Section IV. In the end, the conclusions are drawn in Section V.

## II. NON-CONTACT MEASUREMENT SCHEME

### A. MOIRÉ FRINGE MATHEMATICAL MODEL

Fig. 1 shows the schematic diagram of our scheme for the non-contact measurement of roll angle by using moiré fringes when torsional deformation occurs between two target devices. The setup consists of two parts, i.e., emitting part and receiving part. Two collimators are separately connected with the emitting part and receiving part, and the focal lengths of the two collimators are the same under this scheme. $G_1$ and $G_2$ represent gratings, and are respectively installed in the emitting part and receiving part. The light source, $G_1$, and $G_2$ are fixedly connected to the coaxial line. When torsional deformation occurs, $G_1$ and $G_2$ are driven to rotate synchronously around the $z$-axis. The collimator is an important optical detection instrument, which can simulate the beam from infinity. Parallel beams can be formed when light source passes through the collimating optical system. Thus, non-contact measurement of roll angle can be completed by using this optical path without the aid of intermediate connection structures. Finally, fringe images formed by $G_1$ and $G_2$ are received by charge coupled device (CCD) in the receiving part. Overall, the whole structure is quite flexible, and can realize the non-contact measurement of roll angle conveniently and efficiently.

The Cartesian coordinate system $o$-$xyz$ is established as shown in Fig. 2. The grating system uses the grating pitch as the measurement reference. When the grating pitch is in the range of 10 to 200 $\mu$m, the grating line distance is much larger than the source wavelength. Thus, the diffraction phenomenon can be neglected, and the situation can be analyzed by the occlusion effect of geometric optics [16]. On account of this, the grating pitch should be larger than 10 $\mu$m. Assume the grating pitches of $G_1$ and $G_2$ are $d_1$ and $d_2$ respectively. Take any grating line of $G_2$ as the $y$-axis, its vertical direction as the $x$-axis, and the $z$-axis perpendicular to the $o$-$xy$ plane as the optical axis. Then $\theta$ represents the roll angle between two gratings, and the moiré fringe equation can be obtained based on this coordinate system.

As illustrated in Fig. 2, since the variation of moiré fringes is symmetrically distributed in the angle $\theta \in (0°, 180°)$ and

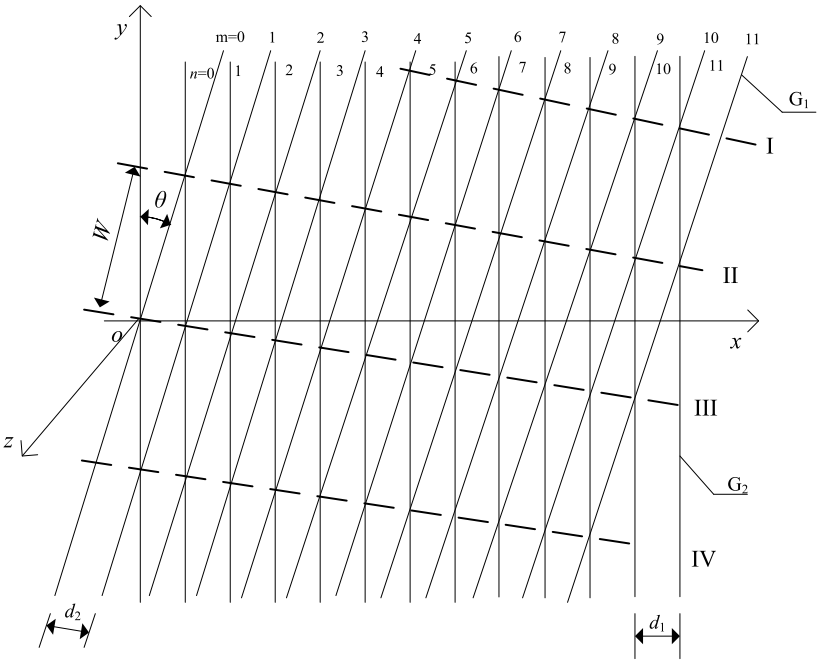


**FIGURE 2.** Moiré fringe space coordinate system.

$\theta \in (180°, 360°)$, the discussion is mainly made in the range of $\theta \in (0°, 180°)$. At first, the grating line equations are established according to the *o-xyz* coordinate system. Let $n$ and $m$ be ordinals of two gratings respectively, and then the equations of the two gratings can respectively be expressed as

$$x = nd_1, \tag{1}$$

$$\begin{cases} x\cos\theta - y\sin\theta = md_2, & \theta \in (0°, 90°) \\ y\sin\theta - x\cos\theta = md_2, & \theta \in (90°, 180°). \end{cases} \tag{2}$$

Thus, the intersection trajectory of the two grating lines can be obtained. As a general case, the intersection line is given by a sequence of $(n, m = n + k)$, where $k = 0, \pm 1, \pm 2$, and so on.

According to the shading effect, the lines I, II, III, and IV are bright stripes of moiré fringes. Now substitute $m = n+k$, $n = x/d_1$ into (2) to solve the general expression of stripes as follows:

$$\begin{cases} y = x\left(1 - \dfrac{d_2}{d_1\cos\theta}\right)\mathrm{ctg}\theta - \dfrac{kd_2}{\sin\theta}, & \theta \in (0°, 90°) \\ y = x\left(1 + \dfrac{d_2}{d_1\cos\theta}\right)\mathrm{ctg}\theta + \dfrac{kd_2}{\sin\theta}, & \theta \in (90°, 180°). \end{cases} \tag{3}$$

Equation (3) is a straight line cluster. Each $k$ value corresponds to a stripe, and the width $W$ of fringe can be given by

$$\begin{cases} W = \dfrac{d_1 d_2}{\sqrt{d_1^2 + d_2^2 - 2d_1 d_2\cos\theta}}, & \theta \in (0°, 90°) \\ W = \dfrac{d_1 d_2}{\sqrt{d_1^2 + d_2^2 + 2d_1 d_2\cos\theta}}, & \theta \in (90°, 180°). \end{cases} \tag{4}$$

In practical sensors, the two gratings have the same pitch $d$. Then the roll angle $\theta$ can be expressed as

$$\begin{cases} \theta = 2\arcsin\dfrac{d}{2W}, & \theta \in (0°, 90°) \\ \theta = 2\arccos\dfrac{d}{2W}, & \theta \in (90°, 180°). \end{cases} \tag{5}$$

Equation (5) indicates that $\theta$ between two gratings can be calculated by measuring the moiré fringe width $W$. Thus, when deformation occurs between the two target devices, the roll angle can be calculated by the changes of the moiré fringe width as follows:

$$\begin{cases} \Delta\theta_m = 2\arcsin\dfrac{d}{2W_2} - 2\arcsin\dfrac{d}{2W_1}, & \theta \in (0°, 90°) \\ \Delta\theta_m = 2\arccos\dfrac{d}{2W_2} - 2\arccos\dfrac{d}{2W_1}, & \theta \in (90°, 180°), \end{cases} \tag{6}$$

where $W_1$ and $W_2$ represent the measured values of the moiré fringe width before and after the deformation, respectively. Since the moiré fringes are symmetrically distributed between 0°–180° and 180°–360°, it is possible to obtain the same width values at the symmetrical positions. These values need to be distinguished by judging the slopes of moiré fringes in the field of view. Compared with other measurement schemes, our proposed scheme does not provide a measurement reference position, and the corresponding roll angle can be calculated based on the changes of the moiré fringe width. Hence, moiré fringes have a good flexibility in measuring the roll angle.

### B. ANALYSIS OF ERROR SOURCES

#### 1) GRATING PERIOD ERROR

According to (5), the measurement accuracy is affected by the grating pitch period error. The limited error of grating line scribe in the manual is $\delta_d = 0.1\mu$m, and it obeys the normal distribution [16], [17]. Then the pitch period RMS error is $\sigma_d = \delta_d/3$ (Further details in Appendix). The measurement error caused by grating scribe can be expressed by

$$\frac{\partial\theta}{\partial d} = \frac{2}{d}\tan\frac{\theta}{2}, \tag{7}$$

$$\sigma_{\theta_d} = \frac{\partial\theta}{\partial d}\sigma_d. \tag{8}$$

#### 2) FRINGE WIDTH ERROR

Equation (5) indicates that the measurement accuracy of roll angle is also related to the fringe width error. The width solution error of moiré fringe is derived from the fitting error of two stripes. Since the CCD image is discontinuous, each stripe may have an error of no more than half of one pixel. Consequently, the fringe width generally has a limit error no more than one pixel. The CCD pixel size used in the instrument is 4.8 $\mu$m * 4.8 $\mu$m. Then, each image data point contains a fitting error of half a pixel ($\delta_W = 2.4\mu$m), which obeys the normal distribution [18], [19]. Thus, the RMS error is $\sigma_W = \delta_W/3$ (Further details in Appendix). The fringe width error can be obtained by

$$\frac{\partial\theta}{\partial W} = \frac{2}{d}\tan\frac{\theta}{2}\sin\frac{\theta}{2}, \tag{9}$$

$$\sigma_{\theta_W} = \frac{\partial\theta}{\partial W}\sigma_W. \tag{10}$$

#### 3) FOCAL LENGTH ERROR

As Fig. 1 demonstrates, in the optical path for non-contact measurement, the accuracy of roll angle is affected by the focal lengths of two collimators. Generally, the focal lengths of two optical systems cannot be exactly equal. The change of the ratio between the two grating images may cause measurement error. Assume the focal length factor is $k$, and then the two grating pitches can be expressed by

$$\begin{cases} d_1 = d \\ d_2 = kd. \end{cases} \tag{11}$$

The manufacturing error $k$ of the collimator focal length in the manual is less than 1%, and the error obeys the uniform distribution [20]. Then the caused error is $\sigma_k = \delta_k/\sqrt{3}$ (Further details in Appendix). The formula of the roll angle transforms as follows:

$$\theta = \arccos\left(\frac{1}{2k} + \frac{k}{2} - \frac{kd^2}{2W^2}\right). \tag{12}$$

Hence, the roll angle measurement error caused by the inconsistent focal length can be calculated as follows:

$$\frac{\partial\theta}{\partial k} = \frac{\left(\frac{1}{2k^2} - \frac{1}{2} + \frac{d^2}{2W^2}\right)}{\sqrt{1 - \left(\frac{1}{2k} + \frac{k}{2} - \frac{kd^2}{2W^2}\right)^2}}, \tag{13}$$

$$\sigma_{\theta_k} = \frac{\partial\theta}{\partial k}\sigma_k. \tag{14}$$

#### 4) ERROR COMPARISON

Fig. 3 provides the corresponding roll angle measurement errors of the above error sources at different angles. Theoretical analysis results indicate that each error source increases rapidly with the increase of the angle range, and that the fringe width error caused by pixel rounding is much larger than the other two. In addition, it can be seen that higher measurement accuracies can be achieved at smaller roll angles [21]. From the above analysis, the measurement accuracy of moiré fringes is significantly affected by various error sources in the system, which follows a power law trend. On this basis, we combine the above characteristics of moiré fringes and propose a novel roll angle measurement scheme.

## III. COMBINED MEASUREMENT SCHEME

### A. MODEL PRINCIPLE

As Section II and related research demonstrate, the methods based on moiré fringes are only suitable for roll deformation measurement in a small angle range [13], [22]. Moreover, when the roll angle is close to 0°, 90°, or 180°, no effective moiré fringes can be obtained in the optical field of view, which limits the robustness and measurement range of these methods. In this paper, we propose to combine the shaft encoder and moiré fringes to solve the problem of limited range and ensure the measurement accuracy. The shaft encoder has an extremely high stability and accuracy, and its error can be ignored [23]. The principle of our scheme is summarized as follows. First, the moiré fringe is adjusted to a small angle position to achieve a high measurement accuracy. Then, the actual roll angle $\Delta\theta$ can be calculated by summing the rotation angle value $\Delta\theta_s$ of the shaft encoder and the measurement value $\Delta\theta_m$ of moiré fringe as follows:

$$\Delta\theta = \Delta\theta_m + \Delta\theta\text{s}. \tag{15}$$

In order to ensure the measurement accuracy of roll angle, this scheme controls the measurement range of moiré fringe within 10′. Here, the measurement range of the predetermined grating rotation angle is selected as 1°30′ –1°40′, and the corresponding moiré fringe width is from 2673.88 to 2406.51 $\mu$m. Notably, the selection of the moiré fringe measurement range is limited by the optical field of view and the size of CCD layout in the system, and the above theoretical error within this range is less than 4″. Finally, by judging the moiré fringe width value, whether the roll angle is within the specified range can be determined. To sum up, the roll angle measurement range by this scheme is not limited, and large range roll measurement values can be achieved by the shaft encoder. At the same time, the moiré fringe can be used to achieve the non-contact measurement of roll deformation and ensure the accuracy in a small roll range.

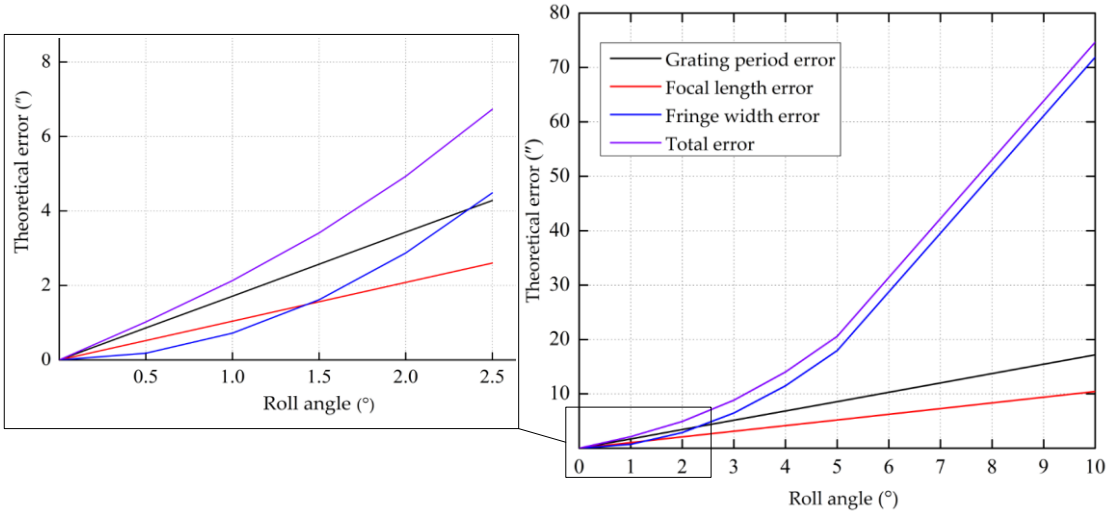


**FIGURE 3.** Variation trends of error sources with roll angle.

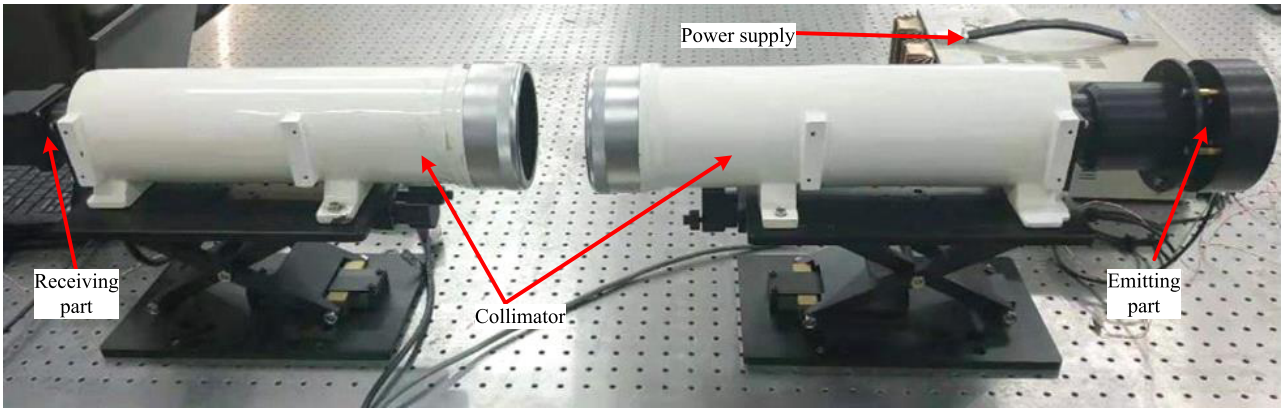


**FIGURE 4.** Experimental equipment layout.

### *B. SENSOR STRUCTURE DESIGN*

Fig. 4 shows the layout of the experimental equipment, and the whole setup of devices is installed on the optical platform. Here, the structure of the emitting part has been further modified and optimized based on that in Fig. 1. The two collimators have the same parameters, so the same grating image can be superimposed on CCD at the focal plane to generate a moiré image. The final image data are processed by computer.

Table 1 lists the main parameters of the system. The CCD used in the experiment has the characteristics of low illumination and high sensitivity, and it can be saturated even if the light source is very weak. When a 5mW red LED is used as the light source, a clear moiré fringe can be obtained. Error analysis in Section II shows that a smaller pixel size of CCD can help extract the center of the moiré fringe and thus reduce the fringe fitting error. The used grating is an isoperiodic circular grating ruler. At present, the common grating pitch in the field of geometric measurement is 20–100 $\mu$m. In this scheme, the grating pitch is selected as 70 $\mu$m. The collimator is a common standard optical detection instrument in the measurement field, and its internal structure is not discussed here. Considering a shorter focal length can acquire a larger optical field of view, which is helpful for the collection of image data, we select a short focal length of 1300 mm for the collimator.

For the receiving part (as shown in Fig. 1), in order to ensure a clear moiré image, the grating should be within the depth of field at the focal length of the collimator, and there should be no gap between CCD and $G_2$. Fig. 5 presents the detailed structural principle of the emitting part. The grating $G_1$, the light source, the rotating mechanism, and the shaft encoder are fixedly connected together, which are coaxial with the collimator. The axes of the two collimators are calibrated by the theodolite to the same axis, and the angle error after calibration is less than $0.5''$. When the target devices at both ends are rolled, the emitting and receiving parts rotate synchronously, and the high-accuracy roll deformation measurement within $10'$ between the two parts can be guaranteed by the moiré fringe. Along with continuous rotation of the rotating mechanism, the moiré fringe width

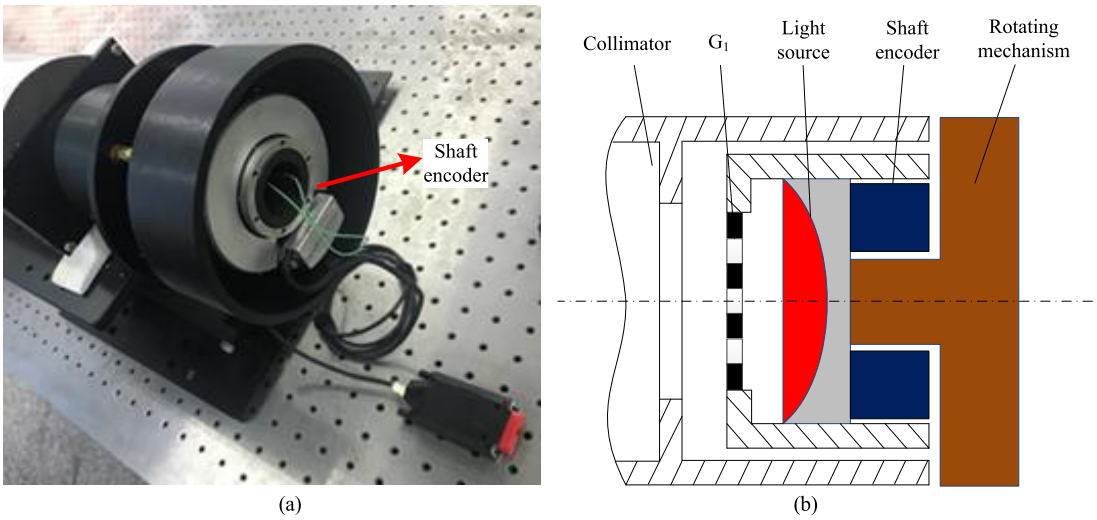


**FIGURE 5.** Structural principle of the emitting part: (a) physical installation and (b) principle structure.

**TABLE 1.** Parameters of the system.

| Parameter | Unit | Value |
|---|---|---|
| Wavelength of the red LED | nm | 625 |
| LED power | mW | 5 |
| Focal length of autocollimator | mm | 1300 |
| Grating pitch | μm | 70 |
| Grating diameter | mm | 10 |
| Pixel size of CCD | μm | 4.8 |
| Resolution of CCD | pixel | 1999×2000 |
| Shaft encoder MRP5080 accuracy | arcsec | ±0.1 |
| Leica theodolite | arcsec | ±0.5 |

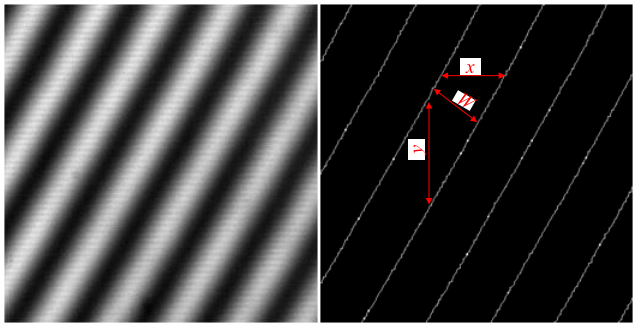


**FIGURE 6.** Moiré fringe image: (a) the original image and (b) extracted center lines.

in the field of view is determined at the same time. When the moiré fringe is adjusted within the predetermined range, the rotation angle of the rotating mechanism is recorded synchronously by the signal acquisition device of the shaft encoder.

## IV. EXPERIMENT

Fig. 6(a) is a captured moiré image, an image processing series, i.e., filtering, contrast enhancement, threshold segmentation, corrosion, and thinning, converts these stripes into single-pixel lines as shown in Fig. 6(b) [24]. If the average horizontal spacing between these lines is denoted as $x$ and vertical spacing as $y$, the width $W$ of moiré fringe can be calculated as follows:

$$W = \frac{x \cdot y}{\sqrt{x^2 + y^2}}. \tag{16}$$

Another shaft encoder is installed to verify the measurement accuracy of our scheme. The operation process of the experimental setup is as follows. First, the control mechanism is rotated to drive $G_1$ and the shaft encoder to rotate, and the generated roll angles can be obtained by the original shaft encoder. Then, the corresponding images are respectively acquired at different angles, and the moiré fringe width is calculated to determine whether the specified range is satisfied. Here the rotation angle 3° of the second encoder is taken as the true value, and the above operation is repeated 10 times to calculate the measurement accuracy. To reduce the effects of random errors, the RMS error of the statistical results is expressed here. As shown in Table 2, the measured value of roll angle is composed of two parts. The value $\Delta\theta_s$ beyond $10'$ is obtained by the feedback signal of the original shaft encoder, and its measurement resolution is less than $\pm 0.1'$. The measured value $\Delta\theta_m$ within $10'$ is mainly calculated by the moiré fringe width.

The RMS error of the statistical results can reach $6.9''$, which guarantees the stable measurement accuracy of our scheme. Compared with the theoretical error analysis model, the actual measurement result is slightly larger than the theoretical value. The shaft encoder has extremely high measurement stability and accuracy, so the measurement error of our scheme mainly comes from the moiré fringe width

**TABLE 2.** Roll angle measurement accuracy within 3°.

| $\Delta\theta_s$ | $\Delta\theta_m$ | Error |
|---|---|---|
| 2°59′28" | 32.8" | -0.8" |
| 2°58′22" | 1′31.1" | 6.9" |
| 2°57′35" | 2′16.4" | 8.6" |
| 2°56′29" | 3′37.5" | -6.5" |
| 2°55′30" | 4′25.1" | 4.9" |
| 2°54′19" | 5′44.8" | -3.8" |
| 2°53′31" | 6′22.3" | 6.7" |
| 2°52′24" | 6′27.6" | 8.4" |
| 2°51′23" | 8′27.7" | 9.3" |
| 2°50′28" | 9′23.6" | 8.4" |
| RMS Error: 6.9" | | |

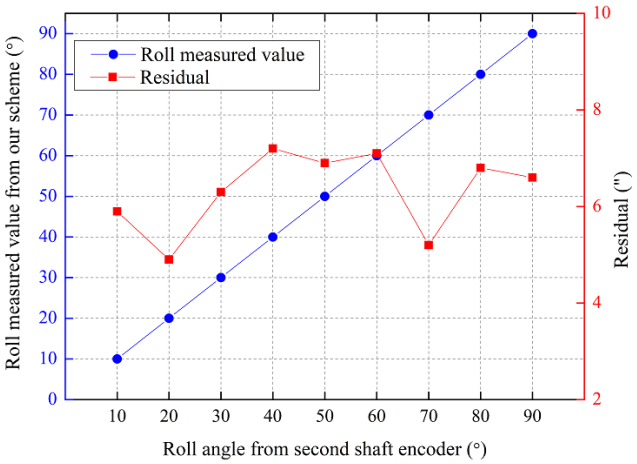


**FIGURE 7.** Roll angle of 0°–90° measurement results.

calculation. For more detailed error analysis, please refer to the error analysis in Section II.

In current engineering applications, the measurement range of roll deformation in most applications is less than 3°, but the moiré fringe is close to 0°, 90°, and other invalid intervals. Specially, in some application occasions, the roll angle may greatly exceed 3°. On account of this, in order to further verify the measurement accuracy and feasibility of the proposed scheme, the measurement range is extended to 0°–90°, and the experimental results are shown in Fig. 7. As can be seen, the measurement error is always kept within 7.8″. Hence, it can be concluded that this scheme has a good measurement stability.

## V. CONCLUSION

In this paper, we propose a novel scheme for roll deformation measurement by combining moiré fringes with the shaft encoder. Moiré fringes can achieve relative roll measurement in a small angle range and do not depend on the system reference datum, thus guaranteeing the measurement accuracy within a small angle range and effectively reducing the impact of system reference errors. Under the help of shaft encoder, the limited measurement angle range of moiré fringes is extended to a large extent, and the measurement accuracy can still be guaranteed. The experimental results demonstrate that the accuracy can reach 6.9″ within 3°, and be better than 7.8″ in the roll range of 0°–90°. Thus it has a good measurement stability. Further, the proposed scheme overcomes the limitations of the imaging characteristics and the field of view of optical system, which can measure any roll angle in the full 360° angular range. Moreover, some modifications are made to improve the overall structure of the system, which can meet the requirements under many non-contact application scenarios.

## APPENDIX

Limit error: It represents the maximum range of errors under a certain probability guarantee. Assuming that the probability that the error of measurement result does not exceed the limit error is $P$, then the probability that the result falls on $1–P$ can be neglected. The limit error is usually expressed by the symbol $\delta_{lim}$.

RMS error: It is also referred as the Standard Deviation, which is used to reflect the degree of dispersion of a data set. The RMS error is commonly expressed as $\sigma$.

According to the knowledge of the probability theory, the two errors have the following relationship:

$$\delta_{\lim\bar{x}} = t\sigma_{\bar{x}}, \tag{A1}$$

where $\bar{x}$ represents the average value of multiple measurement sequences; $t$ represents the confidence factor, which depends on the probability distribution of the data. The common uniform distribution and Gaussian distribution are generally taken as $\sqrt{3}$ and 3, respectively.

## REFERENCES

[1] S. Haris and J. Amdahl, "Analysis of ship–ship collision damage accounting for bow and side deformation interaction," *Mar. Struct.*, vol. 32, pp. 18–48, Jul. 2013.
[2] P. De Girolamo, M. Crespi, A. Romano, A. Mazzoni, M. Di Risio, D. Pasquali, G. Bellotti, M. Castellino, and P. Sammarco, "Estimation of wave characteristics based on global navigation satellite system data installed on board sailboats," *Sensors*, vol. 19, no. 10, p. 2295, May 2019.
[3] S. Zhang, H. Li, T. Zhang, Y. Pang, and Q. Chen, "Numerical simulation study on the effects of course keeping on the roll stability of submarine emergency rising," *Appl. Sci.*, vol. 9, no. 16, p. 3285, Aug. 2019.
[4] X. M. Liu, Y. Y. Zhang, X. Y. Feng, and Q. X. Wang, "A novel method for Hull's three dimensional deformation measurement," *Appl. Mech. Mater.*, vol. 344, pp. 93–98, Jul. 2013.
[5] Y. Lou, L. Yan, B. Chen, and S. Zhang, "Laser homodyne straightness interferometer with simultaneous measurement of six degrees of freedom motion errors for precision linear stage metrology," *Opt. Express*, vol. 25, no. 6, pp. 6805–6821, Mar. 2017.
[6] J. W. Kim, C.-S. Kang, J.-A. Kim, T. Eom, M. Cho, and H. J. Kong, "A compact system for simultaneous measurement of linear and angular displacements of nano-stages," *Opt. Express*, vol. 15, no. 24, pp. 15759–15766, Nov. 2007.
[7] Y. Qiao, C. Wang, X. Li, F. Gao, B. Li, and Y. Li, "Measurement of torsion angular distortion based on moiré fringe," *Opt. Precis. Eng.*, vol. 16, no. 11, pp. 2132–2139, Nov. 2008.
[8] R. Nabergoj and A. Tondl, "Simulation of parametric ship rolling: Effects of hull bending and torsional elasticity," *Nonlinear Dyn.*, vol. 6, no. 3, pp. 265–284, Oct. 1994.

[9] L. Wang, Y. Tang, X. Zhang, and J. Zhang, "Studies on parametric roll motion of ship under wave group by numerical simulation," *Ocean Eng.*, vol. 163, pp. 391–399, Sep. 2018.
[10] E. Plosker, D. Bykhovsky, and S. Arnon, "Evaluation of the estimation accuracy of polarization-based roll angle measurement," *Appl. Opt.*, vol. 52, no. 21, pp. 5158–5164, Jul. 2013.
[11] I. A. Konyakhin and T. V. Turgalieva, "Three-coordinate digital autocollimator," *J. Opt. Technol.*, vol. 80, no. 12, pp. 772–777, Dec. 2013.
[12] T. V. Turgalieva and I. A. Konyakhin, "Autocollimating systems for roll angle measurement of large-scale object deformation," *Proc. SPIE Opt. Metrol.*, vol. 9525, Jun. 2015, Art. no. 952543.
[13] Y. Yin, S. Cai, and Y. Qiao, "Design, fabrication, and verification of a three-dimensional autocollimator," *Appl. Opt.*, vol. 55, no. 35, pp. 9986–9991, Dec. 2016.
[14] J. Jin, L. Zhao, and S. Xu, "High-precision rotation angle measurement method based on monocular vision," *J. Opt. Soc. Amer. A, Opt. Image Sci.*, vol. 31, no. 7, pp. 1401–1407, 2014.
[15] Y. Wei, Z. Ding, H. Huang, C. Yan, J. Huang, and J. Leng, "A non-contact measurement method of ship block using image-based 3D reconstruction technology," *Ocean Eng.*, vol. 178, pp. 463–475, Apr. 2019.
[16] Q. Lv, W. H. Li, Bayanheshig, Y. Bai, Z. Liu, and W. Wang, "Interferometric precision displacement measurement system based on diffraction grating," *Chin. Opt.*, vol. 10, no. 1, pp. 39–50, Feb. 2017.
[17] S. Yokoyama, Y. Hori, T. Yokoyama, and A. Hirai, "A heterodyne interferometer constructed in an integrated optics and its metrological evaluation of a picometre-order periodic error," *Precis. Eng.*, vol. 54, pp. 206–211, Oct. 2018.
[18] A. Belhaoua, S. Kohler, and E. Hirsch, "Error evaluation in a stereovision-based 3D reconstruction system," *EURASIP J. Image Video Process.*, vol. 2010, pp. 1–12, Oct. 2010.
[19] T.-H. Hsieh, P.-Y. Chen, W.-Y. Jywe, G.-W. Chen, and M.-S. Wang, "A geometric error measurement system for linear guideway assembly and calibration," *Appl. Sci.*, vol. 9, no. 3, p. 574, Feb. 2019.
[20] B. Xuan Cao, P. Le Hoang, S. Ahn, J.-O. Kim, H. Kang, and J. Noh, "Measurement of focal length based on laser-beam-spot tracking system using diffractive beam sampler," *Measurement*, vol. 122, pp. 135–140, Jul. 2018.
[21] J. Zhu, S. Hu, X. Su, and Z. You, "Adjustment strategy for inclination Moiré fringes in lithography by spatial frequency decomposition," *IEEE Photon. Technol. Lett.*, vol. 27, no. 4, pp. 395–398, Feb. 15, 2015.
[22] W. Zhu, Y. Lin, Y. Huang, and Z. Xue, "Research on sinusoidal error compensation of Moiré signal using particle swarm optimization," *IEEE Access*, vol. 8, pp. 14820–14831, 2020.
[23] T. Wang, J. Zhao, L. Tian, Y. Yan, L. Yang, C. Chen, Y. Duan, L. Pan, H. Zhao, K. Liu, W. Wan, and Y. Liu, "Influence of parallelism between photoelectric shaft encoder axis and polyhedron one on the rotation angle error," *Infr. Laser Eng.*, vol. 47, no. 2, pp. 234–241, Feb. 2018.
[24] W. Yang, Z. Wang, C. Shen, Y. Liu, S. Liu, Q. Li, W. Du, and Z. Song, "Research on focal length measurement scheme of self-collimating optical instrument based on double grating," *Sensors*, vol. 20, no. 9, p. 2718, May 2020.

**WENCHANG YANG** was born in Shandong, China, in 1992. He received the B.E. degree from the Shandong University of Technology, in 2015. He is currently pursuing the Ph.D. degree with the Changchun Institute of Optics, Fine Mechanics and Physics, Chesse Academy of Sciences, China. His research interests include photoelectric measurement, instrument design, and digital image processing.

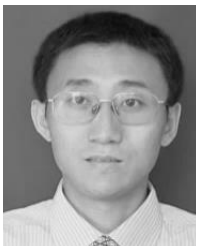

**ZHIQIAN WANG** was born in Jilin, China, in 1969. He received the B.E. and Ph.D. degrees from Jilin University, China, in 1991 and 2009, respectively.

From 2000 to 2010, he was an Associate Professor with the Changchun Institute of Optics, Fine Mechanics and Physics, Chinese Academy of Sciences, China. Since 2010, he has been with the Changchun Institute of Optics, Fine Mechanics and Physics, Chinese Academy of Sciences, where he is currently a Professor with the Department of Optical-Electronic Measurement and a Supervisor of the Ph.D. candidates. He has authored/coauthored more than 40 publications in his areas of research. His main research interests include photoelectric measurement and digital signal processing.

**CHENGWU SHEN** was born in Jilin, China, in 1978. He received the B.E. degree from Jilin University, China, and the M.S. degrees from the Changchun Institute of Optics, Fine Mechanics and Physics, Chinese Academy of Sciences, China, in 2002 and 2006, respectively.

He holds an Associate Research position with the Changchun Institute of Optics, Fine Mechanics and Physics, Chinese Academy of Sciences. His research interests include electronic system design and digital image processing.

**YUSHENG LIU** was born in Sichuan, China, in 1986. He received the B.E. degree from Northeast Normal University, China, and the M.S. degrees from the Changchun Institute of Optics, Fine Mechanics and Physics, Chinese Academy of Sciences, China, in 2008 and 2011, respectively.

He holds an Associate Research position with the Changchun Institute of Optics, Fine Mechanics and Physics, Chinese Academy of Sciences. His research interests include design of optical measurement systems, digital signal processing using DSP, and FPGA implementations.

**SHAOJIN LIU** was born in Jilin, China, in 1979. He received the B.E. degree from the Changchun University of Science and Technology, China, and the Ph.D. degree from the Changchun Institute of Optics, Fine Mechanics and Physics, Chinese Academy of Sciences, China, in 2007.

He holds an Associate Research position with the Changchun Institute of Optics, Fine Mechanics and Physics, Chinese Academy of Sciences. His research interests include visual measurement and optical-electric sensor technologies.